Neutral impurities in tunneling structures

S. K. Kirby, D. Z.-Y. Ting, and T. C. McGill
Thomas J. Watson, Sr., Laboratory of Applied Physics, California Institute of Technology , Pasadena, California 91125
(Received 23 April 1993)

We examine transport in single and double barrier tunneling structures with neutral impurities. For this purpose, we have developed a three-dimensional, tight-binding supercell model of quantum transport capable of simulating potential variations both along the growth direction and in the lateral directions. We find that an isolated attractive impurity in a single barrier can produce a transmission resonance whose position and strength are sensitive to the location of the impurity within the barrier. We also study transmission in the presence of two closely spaced impurities as a function of their separation and orientation relative to the incident plane wave. Multiple impurities can lead to a complex resonance structure that fluctuates widely with impurity configuration. In addition, impurity resonances can give rise to negative differential resistance.

I. INTRODUCTION

State-of-the-art semiconductor manufacturing techniques such as molecular beam epitaxy and nanolithography have given rise to a host of heterostructures that demonstrate new physics and hold technological promise. These nanometer scale devices, such as single and double barrier tunneling structures, operate in the quantum regime, and hence small fluctuations in their structure and composition can affect their characteristics considerably. Impurities, for example, can alter the optical and electrical properties of semiconductor devices. A survey of impurities and other point defects in bulk materials can be found in a review by Pantelides.[1] The electronic structure and electronic levels of neutral impurities have been studied using a number of approaches. Cluster methods, such as the defect molecule model[2] and the atomic cluster model,[3,4] have been used to calculate energy levels of neutral impurities. The extended Hückel theory method, developed by Walter and Birman,[5] has been widely used to calculate electronic states. Self-consistent Green function methods[6] have also been employed. A recent optical study of neutral impurity levels can be found in an article by Monemar.[7] Additional topics such as elastic[8,9] and inelastic[10] scattering from neutral impurities have also been considered.

Only recently have the effects of impurities on transmission in tunneling structures received attention. Resonant tunneling assisted by an energy level associated with a defect has been observed.[11] The authors use a single scattering center calculation and find that negative differential resistance can occur in a single barrier with isolated defects. Double barrier structures with a dilute concentration of impurities in the well have also been considered.[12] An average of the current density over impurity configurations was taken, and it was found that impurities produce a broadening in the well resonance and a reduction in its maximum.

In this paper, we use a tight-binding supercell model which can represent a specific, three-dimensional (3D) configuration of impurities and take interactions between impurities into account. This flexibility allows us to address topics in tunneling in structures with neutral impurities. We find that the particulars of a three-dimensional impurity configuration, such as orientation and inter-impurity distances, play an important role in tunneling. We are thus able to study fluctuations in addition to the average effects of impurities in devices. We find important differences between simulations in one, two, and three dimensions.

In Sec. II we describe the tight-binding supercell model. In Sec. III we apply the model to single and double barrier tunneling structures with neutral impurities. We first examine an isolated impurity in a single barrier. We look at resonance shape and position as a function of material parameters and the location of the impurity within the barrier. We then consider the level splitting and effects on transmission in the case of two closely spaced impurities. We next study three-dimensional distributions of impurities in single and double barrier tunneling structures. We end Sec. III with a current-voltage calculation for a single barrier with an isolated impurity, and we summarize in Sec. IV.

II. METHOD

To model a structure, we employ the one-band, nearest neighbor, cubic lattice tight-binding Hamiltonian

$$H = \sum_{\mathbf{n}} \epsilon_{\mathbf{n}} |\mathbf{n}\rangle\langle\mathbf{n}| - \sum_{<\mathbf{nm}>} t_{\mathbf{nm}} |\mathbf{n}\rangle\langle\mathbf{m}| \,, \tag{1}$$

where the second sum extends over all nearest neighbor pairs on a cubic lattice of lattice constant a. Each of the sites $\mathbf{n}$ is associated with two material parameters: a band edge $E_{\mathbf{n}}$, and an effective mass, $m_{\mathbf{n}}$. In terms of these parameters, the on-site energies $\epsilon_{\mathbf{n}}$ and the hopping matrix elements $t_{\mathbf{nm}}$ used in the Hamiltonian are, following Frensley,[13]

0163-1829/93/48(20)/15237(8)/$06.00

$$\epsilon_{\mathbf{n}} = E_{\mathbf{n}} + \sum_{\mathbf{m}} t_{\mathbf{nm}},$$
$$t_{\mathbf{nm}} = \frac{1}{2}(t_{\mathbf{n}} + t_{\mathbf{m}}), \quad (2)$$
$$t_{\mathbf{n}} = \frac{\hbar^2}{2m_{\mathbf{n}}a^2}.$$

The sum in the first line above is over all nearest neighbor sites $\mathbf{m}$ of site $\mathbf{n}$. These definitions are familiar when one considers the special case of a uniform, bulk material of band edge E_0 and effective mass m, in which case the Hamiltonian gives rise to the band structure

$$E(\mathbf{k}) = E_0 + 2t(3 - \cos k_x a - \cos k_y a - \cos k_z a), \quad (3)$$

where $t = \hbar^2/2ma^2$.

In order to make transport calculations numerically tractable, we apply a supercell scheme to this Hamiltonian. We model a device structure as a series of monolayer planes along the growth direction. Each plane consists of an infinite periodic array of identical rectangular supercells n_x sites in the x direction and n_y sites in the y direction, as in Fig. 1. The sites for the supercell in a particular plane are chosen to reflect the properties of that plane. For example, if the plane represents a region of bulk material, the sites are identical. To represent an impurity in a particular layer, we choose the supercell for that layer to contain a site representing the impurity, and we assign to the other sites the appropriate type of surrounding material. The infinite layers normal to the growth direction are thus modeled by a finite supercell, and a device structure is specified by a finite series of supercells along the growth direction.

To calculate quantum transport in this model, we use an efficient, numerically stable method.[14–16] The transmission coefficients for structures described by the supercell model can be determined by the direct application of the one-dimensional multiband method described by Ting, Yu, and McGill.[16] The basis consists of one orbital for each site in the supercell representation of a structure. The Hamiltonian matrix elements, together with terms representing the boundary conditions in the electrodes, enter into a linear system of equations, which is solved for the electron wave function using an iterative algorithm.[17,18] From this the transmission can be determined.[16]

III. NUMERICAL RESULTS

A. Isolated impurity

We first consider an isolated impurity in a single barrier tunneling structure. We take the electrodes to have a band edge of $E_e = -1$ eV and an effective mass of $m_e = 0.0673m_0$, and the barrier to be nine monolayers thick and to have a band edge of $E_b = 0$ eV and an effective mass of $m_b = 0.1m_0$. The impurity is placed in the middle layer of the barrier. We represent the impurity by a single site with an on-site energy ΔU above that of the barrier, so that $\Delta U < 0$ for an attractive impurity, and $\Delta U > 0$ for a repulsive impurity. The hopping matrix element to the impurity site is the same as that in the rest of the barrier. With the definition $t \equiv \hbar^2/2m_b a^2$ we can take the dimensionless quantity $|\Delta U|/t$ as a measure of impurity strength.

We plot, in Fig. 2, the transmission versus incident electron energy for this structure using a few different values of $\Delta U/t$. For attractive impurities, we see that if $|\Delta U|/t$ is large enough, there will be an impurity level between E_e and E_b. If $|\Delta U|/t$ is not large enough, there will be no impurity level in this range. Nonetheless, the impurity can still affect tunneling, as exhibited by the long-dashed curve. Repulsive impurities have less effect on the transmission, as seen from the curve marked with

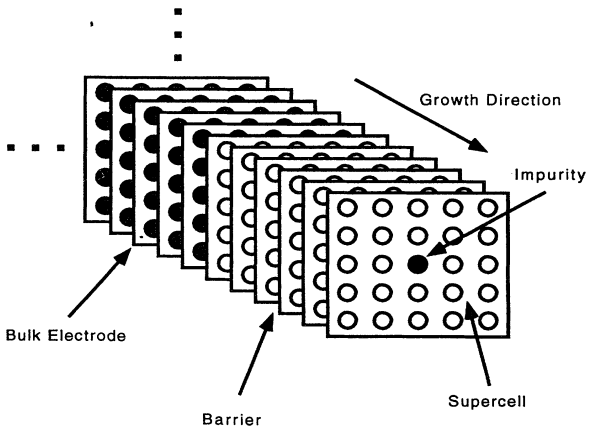

FIG. 1. Supercell representation of an electrode followed by a barrier with an impurity in the sixth barrier plane. The supercells repeat in the planes normal to the growth direction. In the tight-binding model, an on-site energy corresponds to each site, and a hopping matrix element corresponds to each nearest neighbor pair of sites.

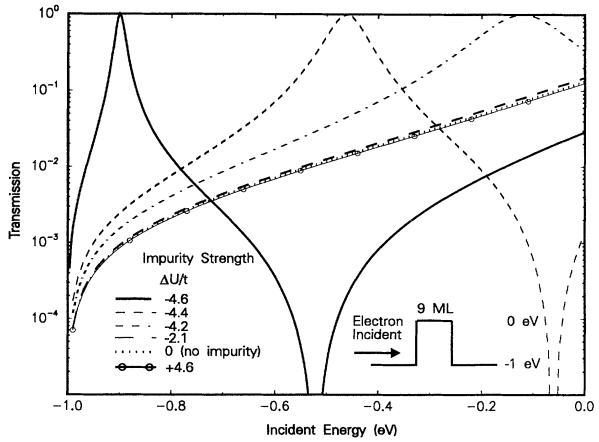

FIG. 2. Isolated impurity in the middle layer of a single barrier tunneling structure. $L_b = 9$ monolayers, 13×13 supercell, $a = 2.825$ Å. $E_b = 0$ eV; $m_b = 0.1m_0$; $E_e = -1$ eV; $m_e = 0.0673m_0$. Various values of $\Delta U/t$ are used. Electrons are incident along the growth direction (i.e., with zero in-plane momentum.)

circles. The higher on-site energy of the repulsive impurities contributes in an averaged sense to an overall slightly higher barrier, thereby reducing transmission. In short we see that an isolated impurity (especially a strongly attractive impurity) can have a significant impact on tunneling.

In addition to a resonance, the transmission coefficient curve for $\Delta U/t=-4.6$ appears to have a zero near $E=-0.52$ eV. This is due to interference caused by repetition of the supercells (and hence impurity sites) in the growth planes. Representing a well isolated impurity would require much larger supercells and a prohibitively large amount of computer memory. Nonetheless, the features we are interested in, namely the resonances, change little for supercells larger than about 13×13, so this size will suffice in most of our calculations.

We have thus far taken full advantage of our model by simulating an impurity in three dimensions. By constructing appropriate supercells, we can also simulate impurities in one and two dimensions. For example, to simulate an impurity in two dimensions, we would use a $1 \times n$ supercell; in one dimension, the supercells would consist of a single site. We use this versatility to show some important differences between tunneling calculations in one, two, and three dimensions. Figure 3 shows the dependence of resonance width and normalized resonance energy E/t on the impurity strength $\Delta U/t$ for a single barrier with an isolated attractive impurity in the middle layer. For a given impurity strength simulations in different dimensions predict different resonance positions and widths. The resonance moves to higher energies as the dimension of the calculation is increased, due to the

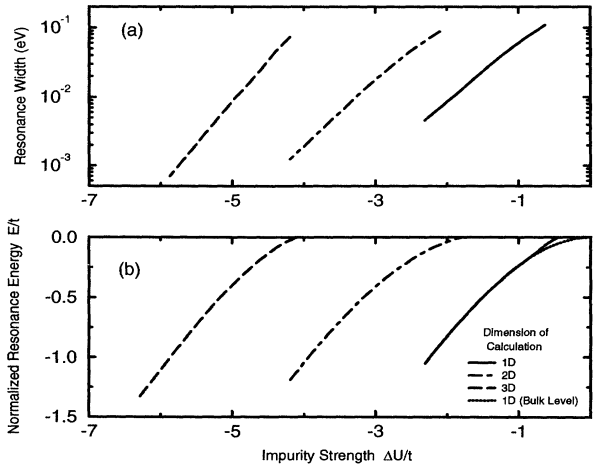

FIG. 3. Resonance widths and normalized resonance energies E/t for an isolated impurity in the middle barrier layer of a single barrier as calculated in one, two, and three dimensions. The dotted curve is the analytical result for the resonance position of a single impurity in a bulk 1D sample. $L_b = 9$ monolayers, 1×1, 1×10, and 10×10 supercells are used in 1D, 2D, and 3D respectively, $a = 2.825$ Å. $E_b = 0$ eV; $m_b = 0.1m_0$; $m_e = 0.0673m_0$. Various electrode band edges $E_e \leq -1$ eV were chosen so that E_e was below the resonance level. Electrons are incident along the growth direction.

increasing number of directions in which the impurity bound state is confined. In one-dimensional simulations, it is confined only along the growth direction, whereas in three-dimensional simulations, it is confined in the lateral directions as well. When the resonance level rises, confinement along the growth direction grows weaker, due to the finite barrier thickness. Thus, as the dimensionality increases and the resonance level rises, the resonance width increases, as in the top panel of Fig. 3.

The finite thickness of the barrier can also affect the resonance position. For a strongly attractive impurity, the resonance position in a single barrier agrees with the level of the impurity in a bulk sample of barrier type material. In one dimension the bulk level is[19]

$$E/t = 2 - \sqrt{4 + \Delta U^2/t^2}, \tag{4}$$

and at high values of $|\Delta U|/t$, this agrees with the resonance position of an impurity in a single barrier. For weaker impurities, however, the single barrier resonances are at energy levels different from those of impurities in bulk samples (see Fig. 3.) Although a bound level always exists in bulk in one and two dimensions for $\Delta U/t < 0$,[20] no such level exists for weak impurities in a single barrier of finite thickness. The finite extent along the growth direction does not support a bound state for very weakly attractive impurities.

These results on resonance position and width can be used to predict how neutral impurities might affect transmission in a single barrier. Whenever the impurity level lies above E_e, a transmission resonance can be expected. In this regard, we stress the important differences in the predictions of the one-, two-, and three-dimensional simulations. We also stress the importance of the finite barrier thickness in determining the resonance widths and positions, especially for weak impurities. Finally, as we saw earlier, even when there is no bound level between E_e and E_b, a neutral impurity can still affect transmission in this energy range.

B. Resonance shape

In addition to impurity strength, the impurity location also impacts transmission. As an impurity is moved along the growth direction in a single barrier, the transmission resonance it produces changes shape and position. In Fig. 4 we plot resonance position, resonance width, and the maximum transmission coefficient as a function of impurity location in a 22 monolayer thick barrier. We find that the resonance moves to slightly higher energy as the impurity approaches the center of the barrier due to increasing confinement — the impurity site is surrounded by thicker walls. We find that the resonance width decreases as the impurity is moved toward the center of the barrier, another sign of increasing isolation from the electrodes. The maximum transmission increases to unity as the impurity approaches the middle layer of the barrier. It is clear that the maximum transmission increases faster than the resonance width decreases, so the transmission resonance grows stronger as the impurity moves

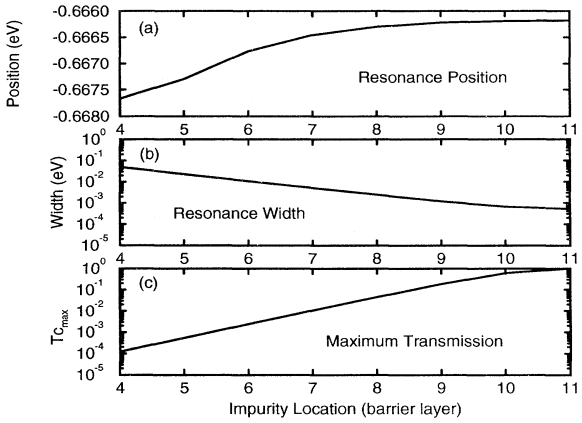

FIG. 4. Resonance shape as a function of impurity location along the growth direction. The horizontal axis is labeled with the number of the barrier layer in which the impurity resides. The plot begins at layer 4, since the resonance shape is difficult to measure when the impurity is closer to the electrode. $L_b = 22$ monolayers, 13×13 supercell, $a = 2.825$ Å. $E_b = 0$ eV, $m_b = 0.1m_0$, $E_e = -1$ eV, $m_e = 0.0673m_0$, $\Delta U/t = -4.5$. Electrons are incident along the growth direction. Resonance width is the width at half maximum.

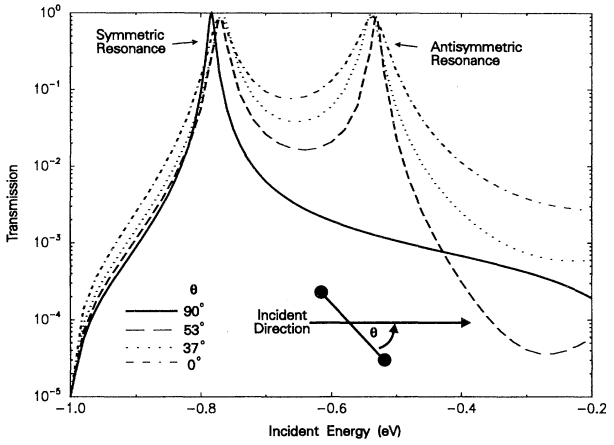

FIG. 5. Transmission vs incident energy for a single barrier with two impurities separated by five lattice spacings. The plane wave is incident along the growth direction (z axis) which makes angle θ with the impurity separation direction. The midpoint between the impurities lies in the middle of the barrier. $L_b = 13$ monolayers, 13×13 supercell, $a = 2.825$ Å. $E_b = 0$ eV, $m_b = 0.1m_0$, $E_e = -1$ eV, $m_e = 0.0673m_0$, $\Delta U/t = -4.5$.

toward the middle layer of the barrier. From this we might expect that attractive impurities near the center of a barrier would play a larger role in the transmission than those near the edges. In any event, both the resonance strength and position depend on the location of the impurity within the barrier.

C. Two impurities

Having studied a single impurity, we now turn to the case of two attractive impurities. The interaction of two closely spaced impurities gives rise to a level splitting. The lower energy level corresponds to a state which is symmetric along the direction of separation of the impurities, and the higher energy level corresponds to an antisymmetric state. Each of these levels can result in a transmission resonance, depending upon the direction of the incident plane wave relative to the direction of separation of the two impurities. Whenever the direction of the incident plane wave has a component along the direction of separation of the two impurities, resonant tunneling can occur via both the symmetric and antisymmetric levels. When the two directions are orthogonal, however, resonant tunneling can occur only via the symmetric level.

To illustrate this we examine the transmission through a single barrier with two impurities separated by five lattice spacings. We plot the transmission coefficient versus energy for different relative orientations of the impurity separation direction and the incident direction. In Fig. 5, the direction of the incident plane wave is fixed along the growth direction (z axis), and the impurity separation vector makes angle θ with this direction. The midpoint between the two impurities lies in the middle of the barrier. We note that for $\theta = 90°$, i.e., the incident and separation directions are orthogonal, resonant tunneling occurs only via the symmetric level. As θ decreases, and the component of the incident plane wave direction along the separation direction increases, the resonance associated with the antisymmetric level increases in strength. The resonance widths of both the symmetric and antisymmetric resonances increase as θ decreases, since the impurities are moved closer to the electrode-barrier interfaces. In Fig. 6, we keep the impurity locations fixed

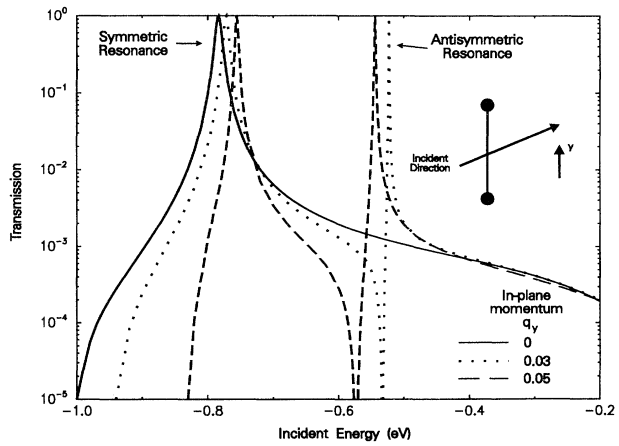

FIG. 6. Transmission vs incident energy for a single barrier with two impurities separated by five lattice spacings along the y direction in the middle barrier layer. The incident in-plane momentum q_y (measured in units of π/a) is varied. $L_b = 13$ monolayers 13×13 supercell, $a = 2.825$ Å. $E_b = 0$ eV, $m_b = 0.1m_0$, $E_e = -1$ eV, $m_e = 0.0673m_0$, $\Delta U/t = -4.5$.

at a separation of five lattice spacings along the y direction in the middle plane of the barrier, and we vary the incident direction. As the in-plane momentum (along the separation direction) q_y is increased, the antisymmetric resonance again grows stronger. The small variations in resonance positions stem from the in-plane momentum energy shift as well as from finite supercell size effects. Thus the relative orientation of the incident direction and the impurity separation direction can play a significant role in the transmission properties of a tunneling structure.

Having examined orientation dependence, we next study level splitting as a function of impurity separation. We find that the level splitting decreases as the impurities are moved further apart. This is due to decreasing interaction between the impurities. Figure 7 shows the wave function in a single barrier with two closely spaced impurities. The system exhibits two bound levels, and the magnitude of the wave function along the line of the impurities is plotted at the symmetric state level. This clearly demonstrates the exponential decrease in the wave function magnitude with distance from the impurities, which causes the level splitting to decrease as the impurities are moved further apart.

We now study the level splitting as a function of impurity separation. We simulate transmission through a single barrier with two closely spaced impurities in one, two, and three dimensions and measure resonance level splitting as a function of impurity separation distance. In two and three dimensions, we are able to measure the splitting for different orientations of the impurity separation direction relative to the underlying square and cubic lattices. We find that, in all cases, the level splitting drops off exponentially with increasing distance between impurities along a given direction (see Fig. 8). The splitting is not the same in all directions, however, for a given

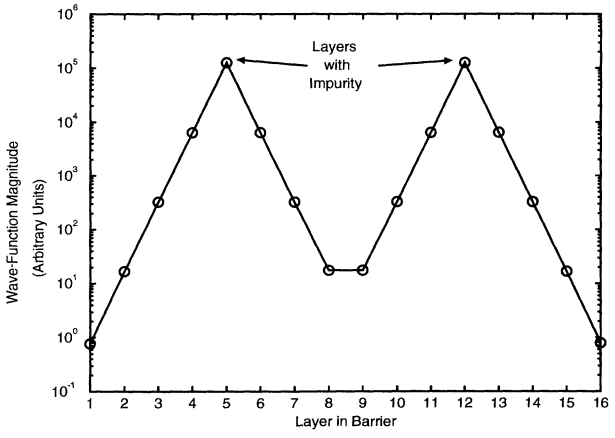

FIG. 7. Symmetric state wave function magnitude along the line joining two impurities separated by seven lattice spacings along the growth direction in a single barrier. (A line is drawn to guide the eye.) $L_b = 16$ monolayers, 10×10 supercell, $a = 2.825$ Å. $E_b = 20$ eV, $m_b = 0.477m_0$, $E_e = 0$ eV $m_e = 0.0673m_0$, $\Delta U/t = -20$. Electrons are incident along the growth direction.

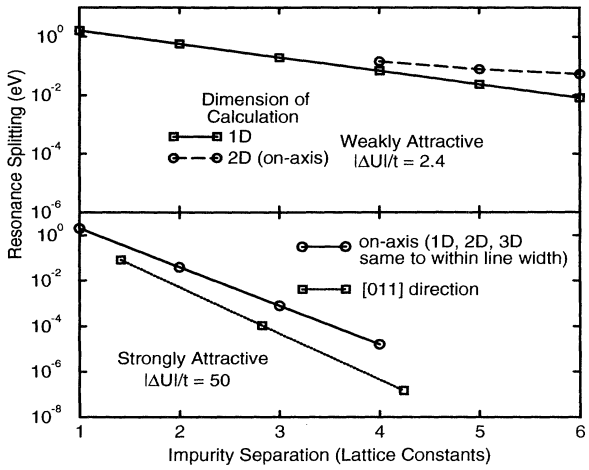

FIG. 8. Resonance splitting as a function of impurity separation. For weakly attractive impurities separated along an axis (top panel) the splitting is different in one and two dimensions; for strongly attractive impurities (bottom panel) it is the same in one, two, and three dimensions. Splitting also depends on the orientation of the impurity pair within the lattice. $L_b = 26$ monolayers, 1×1, 1×15 and 15×15 supercells used for 1D, 2D, and 3D, respectively, $a = 2.825$ Å. $m_b = 0.477m_0$, $m_e = 0.0673m_0$. In the top panel, $E_b = 0$ eV, $E_e = -2.4$ eV. In the bottom panel, $E_b = 50$ eV, $E_e = 0$ eV. Electrons incident along the growth direction.

separation distance. In the bottom panel of Fig. 8, we plot splitting versus separation for impurities separated along a cubic lattice axis (on axis) as well as along the [011] direction. Not only is the splitting different in the two directions for a given separation distance, but it also drops off at a different exponential rate. When we calculate the splitting versus separation for impurities placed on axis, the result is different when calculated in different dimensions unless the impurities are very strongly attractive. The top panel shows that the splitting is different in one and two dimensions for $|\Delta U|/t = 2.4$. In the bottom panel, $|\Delta U|/t = 50$, and the splitting is the same in one, two, and three dimensions. The reason that the splitting for very strongly attractive impurities separated along a cubic lattice axis is the same in one, two, and three dimensions is that the overlap of wave functions localized at the impurity sites is nearly the same in the three dimensions.

For the range of parameters we have chosen in Fig. 8, we see that when impurities are separated by more than three lattice constants, the splitting should be negligible. When spaced closely, however, interimpurity interactions can play a major role in determining resonance positions. In this case, the orientation of the impurity pair in the lattice should be taken into account. Thus there are several factors that determine the resonance structure to which an impurity distribution gives rise. For isolated impurities, the location within the barrier plays the dominant role in determining the resonance positions and strengths. For pairs of closely spaced impurities, interimpurity distance and orientation play the leading role.

Based on these results, summarized in Figs. 4, 5, and 8, we might expect that the shape of the transmission coefficient curve should fluctuate widely with configuration in a single barrier with a high concentration of impurities, where both impurity location and interactions are important.

D. Multiple impurities

We examine a single barrier with a random distribution of attractive impurities. We calculate transmission for two different configurations of four impurities placed randomly among the sites of the nine layers of 20×20 supercells representing the barrier. Figure 9 contains the results. Comparing with the transmission coefficients for an impurity-free single barrier, we see that the impurities give rise to several resonances of varying strengths and positions. Note also that the shape of the transmission coefficient curve is indeed very different for the two configurations.

Impurities in double barrier structures also affect transmission, as illustrated in Fig. 10. We consider first the case of impurities in the well and then the case of impurities in the barriers. The top panel of Fig. 10 shows the transmission coefficient curves for different concentrations of attractive impurities in the well. The lower on-site energy of these attractive impurities contributes in an averaged sense to a lower effective well band edge. As the impurity concentration is increased, this effective band edge moves down, and the $n = 1$ well resonance shifts down. In addition, the impurities in the well can give rise to new resonances, as shown by the solid curve.

The bottom panel of Fig. 10 shows the transmission in a double barrier structure with attractive impurities in the barriers. Just as in the case with impurities in the well, attractive impurities in the barrier can lower

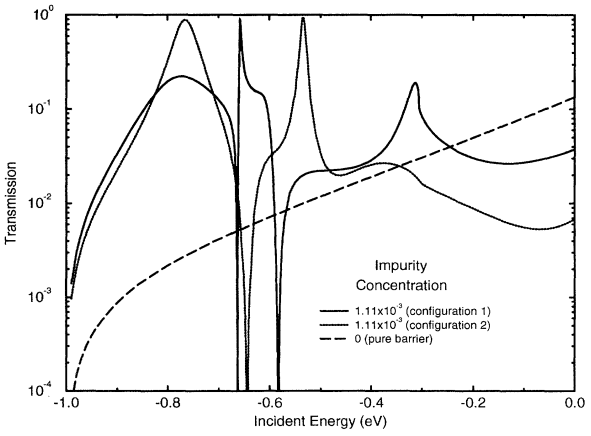

FIG. 9. Single barrier with multiple impurities. $L_b = 9$ monolayers, 20×20 supercell, $a = 2.825$ Å. $E_b = 0$ eV, $m_b = 0.1m_0$, $E_e = -1$ eV, $m_e = 0.0673m_0$, $\Delta U/t = -4.5$. Impurity concentration is $c = 1.11 \times 10^{-3}$ (four impurities were distributed at random among the $9 \times 20 \times 20$ sites of the barrier). Transmission coefficients are shown for two different configurations. Electrons incident along the growth direction.

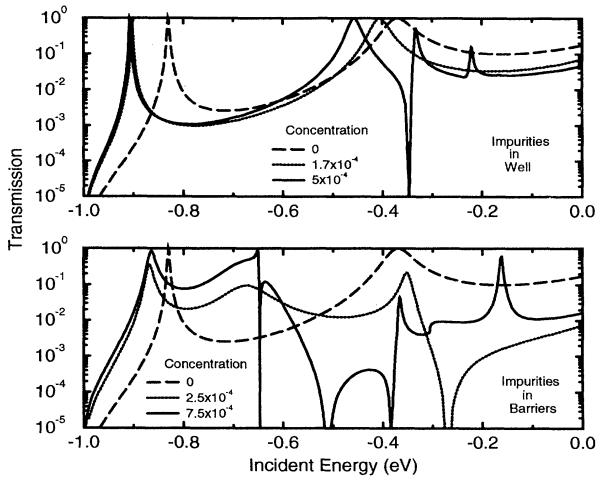

FIG. 10. Double barrier with multiple impurities. $L_b = 5$ monolayers, $L_w = 15$ monolayers, 20×20 supercell, $a = 2.825$ Å. $E_b = 0$ eV, $m_b = 0.1m_0$, $E_e = -1$ eV, $m_e = 0.0673m_0$, $\Delta U/t = -4.5$. For the case of impurities in the well, ΔU still refers to the difference between the impurity on-site energy and that of the barrier. The top panel shows the case of impurities in the well, and the bottom panel shows the case of impurities in the barriers. Electrons incident along the growth direction.

the effective barrier edge. This leads to a lowering and broadening of the $n = 1$ well resonance as seen in the figure. Again we notice new resonances of various strengths and positions.

In both single and double barrier structures, we have seen that impurities can give rise to resonances. The supercell size in the above calculations, 20×20, implies a cross-sectional area approximately 5.7 nm on an edge. To simulate transport through a larger region of a device, we would need to perform configuration averaging over a large number of different impurity distributions. With a high impurity concentration, the wide variation in resonance structure for different local configurations as in Fig. 9 would no longer allow impurities to produce distinct resonances when probed over a large area. Impurities would, however, still contribute collectively to the transmission by shifting and broadening well resonances in a double barrier or by increasing overall transmission in a single barrier, for example.

E. Current-voltage calculation

Thus far we have examined the effects of impurities on the transmission coefficients of tunneling devices. We have seen that impurities can shift and broaden resonances. Just as importantly, however, when probing devices over a small area, such as with scanning probe microscopy, impurities can give rise to new resonances. These resonances have important consequences for current-voltage characteristics in that they could give rise to negative differential resistance. Experimental evidence of negative differential resistance due to a locally

favorable current path created by a donor in the well of double barrier has been presented.[21]

We give here the results of our supercell calculation of the 0 K current-voltage characteristic of a single barrier with an attractive impurity in the middle layer. We use the same material parameters as in Sec. III A. The barrier is nine monolayers thick, and we take the Fermi level in the electrodes to be 0.05 eV above the band edge. In Fig. 11 we plot the current density versus applied bias for this device. We see that the isolated impurity gives rise to substantial peak current and negative differential resistance as a result of resonant tunneling via the impurity level.

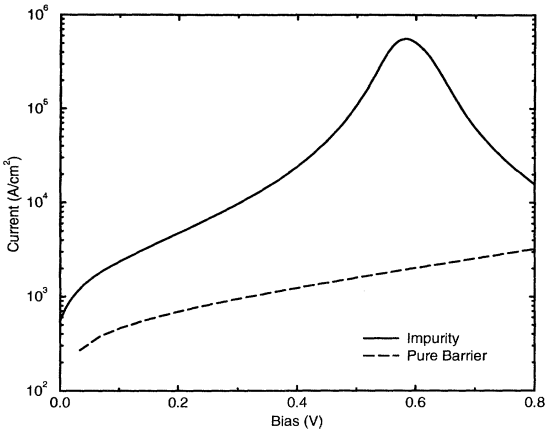

FIG. 11. Negative differential resistance in a single barrier with an isolated impurity in the middle barrier layer. $L_b = 9$ monolayers, 13×13 supercell, $a = 2.825$ Å. $E_b = 0$ eV, $m_b = 0.1m_0$, $E_e = -1$ eV, $m_e = 0.0673m_0$, $\Delta U/t = -4.5$. Electrode Fermi level is 0.05 eV above the electrode band edge. Calculated at 0 K. Also shown for comparison is the current-voltage characteristic of a pure single barrier with the same parameters.

IV. CONCLUSION

We have explored several ways in which neutral impurities can play an important role in quantum transport in tunneling devices. For this purpose, we have developed an efficient, numerically stable method for calculating quantum transport in three dimensions. We have found that an isolated impurity can give rise to a transmission resonance. We have investigated the variation of resonance shape and position with the location of an impurity in a single barrier and found that the resonance moves to higher energy, and that the resonance strength grows as the impurity is moved toward the center of the barrier. We have studied the interaction of two closely spaced impurities and found that the manifestation of level splitting in the transmission depends on the relation between the incident electron direction and the impurity separation direction. We have also seen how the level splitting is different when calculated in different dimensionalities, unless the impurities are strongly attractive. An analysis of single and double barriers with multiple impurities reveals that strongly attractive impurities can have a substantial impact on transmission. Depending on impurity concentration and the area over which a structure is probed, the impurities can shift and broaden resonances in a double barrier and increase overall transmission in a single barrier or give rise to new resonances. The influence of impurities thus depends on many factors including material parameters, location, distribution, and concentration. In many situations, three-dimensional simulation is essential to understanding the physical phenomena for which the impurities are responsible.

ACKNOWLEDGMENTS

The authors would like to thank Dr. Eric F. Van de Velde and Professor Steven E. Koonin for helpful discussion. S. K. Kirby would like to thank the Office of Naval Research (ONR) for support during this work. This work was also supported by the Office of Naval Research under Grant No. N00014-89-J-1141.

[1] S. T. Pantelides, Rev. Mod. Phys. **50**, 797 (1970).
[2] C. A. Coulson and M. J. Kearsely, Proc. R. Soc. London Ser. A **241**, 433 (1957).
[3] R. P. Messmer and G. D. Watkins, Phys. Rev. B **7**, 2568 (1973).
[4] L. U. Dong and L. U. Fen, Chin. Phys. **1**, 472 (1981).
[5] D. G. Thomas, *II-VI Semiconducting Compounds* (Benjamin, New York, 1967).
[6] M. Scheffler, J. Bernholc, N. O. Lipari, and S. T. Pantelides, Phys. Rev. B **29**, 3269 (1984).
[7] B. Monemar, H. P. Gislason, and W. M. Chen, Phys. Rev. B **33**, 4424 (1986).
[8] K. C. Wong, J. Callaway, N. Y. Du, and R. A. LaViolette, Phys. Rev. B **43**, 1576 (1991).
[9] T. C. McGill and R. Baron, Phys. Rev. B **11**, 5208 (1975).
[10] K. C. Wong, N. Y. Du, J. Callaway, and R. A. LaViolette, Phys. Rev. B **41**, 12 666 (1991).
[11] D. Stievenard, X. Letartre, and M. Lannoo, Appl. Phys. Lett. **61**, 1582 (1992).
[12] V. I. Sugakov and S. A. Yatskevich, Fiz. Tverd. Tela (Leningrad) **33**, 529 (1991) [Sov. Phys. Solid State **33**, 302 (1991)].
[13] W. R. Frensley, Rev. Mod. Phys. **62**, 745 (1990).
[14] C. S. Lent and D. J. Kirkner, J. Appl. Phys. **67**, 6353 (1990).
[15] W. R. Frensley (private communication).
[16] D. Z.-Y. Ting, E. T. Yu, and T. C. McGill, Phys. Rev. B **45**, 3583 (1992).
[17] Roland W. Freund and Noel M. Nachtigal, *QMR: a Quasi-Minimal Residual Method for Non-Hermitian Linear Systems,* RIACS, NASA Ames Research Center (to be published, in Numerische Mathematik).

[18] E. F. Van de Velde (unpublished).
[19] R. P. Feynman, R. B. Leighton, and M. Sands, *The Feynman Lectures on Physics* (Addison-Wesley, Menlo Park, 1965).
[20] E. N. Economou, *Green's Functions in Quantum Physics* (Springer-Verlag, New York, 1967).
[21] M. W. Dellow, P. H. Beton, C. J. G. M. Langerak, T. J. Foster, P. C. Main, L. Eaves, M. Henini, S. P. Beaumont, and C. D. W. Wilkinson, Phys. Rev. Lett. **68**, 1754 (1992).